

Further modeling of q_{95} windows for the suppression of edge localized modes by resonant magnetic perturbations in the DIII-D tokamak

Cite as: Phys. Plasmas **28**, 022503 (2021); <https://doi.org/10.1063/5.0035874>

Submitted: 31 October 2020 . Accepted: 12 January 2021 . Published Online: 02 February 2021

 R. Fitzpatrick

COLLECTIONS

 This paper was selected as an Editor's Pick



View Online



Export Citation



CrossMark

ARTICLES YOU MAY BE INTERESTED IN

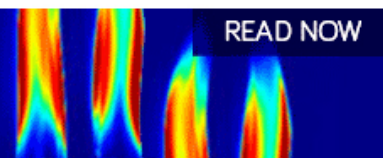
[Predicting nonresonant pressure-driven MHD modes in equilibria with low magnetic shear](#)
Physics of Plasmas **28**, 012106 (2021); <https://doi.org/10.1063/5.0032489>

[First observation of increased DT yield over prediction due to addition of hydrogen](#)
Physics of Plasmas **28**, 012707 (2021); <https://doi.org/10.1063/5.0030852>

[Evidence of \$E \times B\$ staircase in HL-2A L-mode tokamak discharges](#)
Physics of Plasmas **28**, 012512 (2021); <https://doi.org/10.1063/5.0022679>

AIP Advances
Fluids and Plasmas Collection

READ NOW



Further modeling of q_{95} windows for the suppression of edge localized modes by resonant magnetic perturbations in the DIII-D tokamak

Cite as: Phys. Plasmas **28**, 022503 (2021); doi: [10.1063/5.0035874](https://doi.org/10.1063/5.0035874)

Submitted: 31 October 2020 · Accepted: 12 January 2021 ·

Published Online: 2 February 2021




View Online



Export Citation



CrossMark

R. Fitzpatrick^{a)} 

AFFILIATIONS

Department of Physics, Institute for Fusion Studies, University of Texas at Austin, Austin, Texas 78712, USA

^{a)} Author to whom correspondence should be addressed: rfitzp@farside.ph.utexas.edu

ABSTRACT

An improved resonant plasma response model that more accurately captures the physics of the interaction between a tokamak plasma and a resonant magnetic perturbation (RMP) is developed. The model interpolates between the linear and the nonlinear response regimes and takes into account the fact that the slip-frequency is non-zero in the nonlinear regime. The improved model is incorporated into the extended perturbed equilibrium code (EPEC) toroidal asymptotic matching code. The modified EPEC code is used to investigate RMP-induced edge-localized-mode (ELM) suppression in DIII-D H-mode discharge #145380. Somewhat surprisingly, allowing for a finite slip-frequency (i.e., relaxing the so-called no-slip constraint) is found to only slightly facilitate the locking of driven magnetic island chains to the RMP, and, hence, to only slightly facilitate RMP-induced ELM suppression. This is true despite the fact that the nature of non-locked island solutions is radically different when the no-slip constraint is imposed compared to when it is relaxed (in the first case, the widths of the island chains driven at the rational surfaces pulsate, and in the second case, they remain steady). The previously obtained conclusion that the response of a typical H-mode tokamak plasma to an RMP cannot be accurately modeled by linear theory is confirmed. The previously obtained conclusion that the best agreement between theory and observations is achieved by assuming that the natural frequencies of tearing modes, in the absence of the RMP, are determined by the local equilibrium $\mathbf{E} \times \mathbf{B}$ velocity is also confirmed.

Published under license by AIP Publishing. <https://doi.org/10.1063/5.0035874>

I. INTRODUCTION

In the context of tokamak plasmas, a resonant magnetic perturbation (RMP) refers to an externally generated, (usually) static, helical magnetic perturbation that resonates at one or more “rational” magnetic flux-surfaces within the plasma. Resonant magnetic perturbations have been successfully employed to compensate error fields (i.e., accidentally produced RMPs) and, thereby, to prevent the associated formation of locked modes, in a wide variety of different types of tokamak discharge.^{1–3} RMPs have also been successfully used to either mitigate or completely suppress edge-localized-modes (ELMs) in H-mode tokamak discharges.^{4–9}

“Asymptotic matching” is by far the most efficient method for modeling the response of a tokamak plasma to an RMP.^{10–20} According to the asymptotic matching approach, the response of the plasma to the applied RMP is governed by a combination of flux-freezing and perturbed force balance—this combination is usually referred to as “marginally stable ideal-magnetohydrodynamics (MHD)” —everywhere in the plasma apart from a number of relatively

narrow (in the radial direction) regions in which the applied perturbation resonates with the equilibrium magnetic field. Magnetic reconnection can take place within the resonant regions to produce relatively narrow magnetic island chains. Within the resonant regions, the plasma response is governed by linear or nonlinear two-fluid resistive-MHD, depending on whether the induced magnetic island widths are smaller or larger, respectively, than the corresponding linear layer widths. Thus, when employing the asymptotic matching approach, the equations of marginally stable ideal-MHD are solved in the so-called “outer region” that comprises most of the plasma (and the surrounding vacuum), the equations of linear/nonlinear two-fluid resistive-MHD are solved in the various resonant layers that constitute the so-called “inner region,” and the two sets of solutions are then asymptotically matched to one another.

In the nonlinear resonant response regime, the evolution of the island chain width in a given resonant layer is governed by the familiar “Rutherford island width evolution equation.”^{12,21} On the other hand, the phase evolution of the island chain is conventionally governed by

the well-known “no-slip constraint.”¹⁵ According to this constraint, plasma is trapped inside the magnetic separatrix of the island chain, which forces the chain to co-rotate with the local plasma flow. In reality, however, the plasma is able to diffuse resistively across the separatrix to some extent.^{22,23}

The recently developed, toroidal, asymptotic matching code EPEC (extended perturbed equilibrium code) has been used to simulate RMP-induced ELM suppression in DIII-D H-mode plasmas.^{24,25} The original EPEC model incorporates the no-slip constraint. The first aim of this paper is to investigate whether improving the resonant response component of the EPEC model by relaxing the no-slip constraint leads to better agreement with experimental results. The second aim is to examine whether improving the manner in which the resonant plasma response component of the EPEC model interpolates between the linear and the nonlinear regimes gives rise to better agreement with experimental results.

II. CYLINDRICAL RESONANT RESPONSE MODEL

A. Introduction

For the sake of simplicity, and also to make a better connection with previous research, let us commence our investigation by discussing the resonant response of a tokamak plasma to an RMP in cylindrical geometry.

B. Plasma equilibrium

Consider a large aspect-ratio, low- β , circular cross section, tokamak plasma. Such a plasma is well approximated as a periodic cylinder. Suppose that the minor radius of the plasma is a . Standard cylindrical coordinates (r, θ, z) are adopted. The system is assumed to be periodic in the z -direction, with periodicity length $2\pi R_0$, where $R_0 \gg a$ is the simulated plasma major radius. It is convenient to define the simulated toroidal angle $\phi = z/R_0$. The equilibrium magnetic field is written $\mathbf{B} = [0, B_\theta(r), B_\phi]$. The so-called “safety-factor,” $q(r) = r B_\phi / (R_0 B_\theta)$, parameterizes the helical pitches of equilibrium magnetic field-lines.

C. Plasma response to RMP

Consider the response of the plasma to an externally generated, static, helical, RMP. Suppose that the RMP has m periods in the poloidal direction and n periods in the toroidal direction. It is convenient to express the perturbed magnetic field and the perturbed plasma current density in terms of a perturbed poloidal magnetic flux (divided by $2\pi R_0$), $\psi(r, \theta, \phi, t)$. In fact, $\delta\mathbf{B} = \nabla\psi \times \nabla z$, where $\psi(r, \theta, \phi, t) = \hat{\psi}(r, t) \exp[i(m\theta - n\phi)]$, and $\hat{\psi}$ is real. This particular representation is valid provided that $m/n \gg a/R_0$.¹⁵

The response of the plasma to the RMP is governed by the equations of marginally stable, ideal-MHD everywhere in the plasma, apart from a relatively narrow (in r) region in the vicinity of the so-called “rational surface,” minor radius r_s , at which $q(r_s) = m/n$.¹⁵

It is convenient to parameterize the RMP in terms of the so-called “vacuum magnetic flux,” $\Psi_v(t) = |\Psi_v| e^{-i\varphi_v}$, which is defined to be the value of $\hat{\psi}(r, t)$ at radius r_s in the presence of the RMP, but in the absence of plasma. Here, φ_v is the helical phase of the RMP. Likewise, the response of the plasma in the vicinity of the rational surface is parameterized in terms of the so-called “reconnected magnetic

flux,” $\Psi_s(t) = |\Psi_s| e^{-i\varphi_s}$, which is the actual value of $\hat{\psi}(r, t)$ at radius r_s . Here, φ_s is the helical phase of the reconnected magnetic flux.

The intrinsic stability of the m, n tearing mode is governed by the dimensionless parameter $E_{ss} = [d\hat{\psi}_s/d\ln r]_{r_s}^{r_{s+}}$, where $\hat{\psi}_s(r)$ is a solution of the marginally stable, ideal-MHD equations, for the case of an m, n helical perturbation, which satisfies physical boundary conditions at $r=0$ and $r=a$, in the absence of the RMP, and is such that $\hat{\psi}_s(r_s) = 1$.^{10,16} According to resistive-MHD theory,^{10,12} if $E_{ss} > 0$, then the m, n tearing mode spontaneously reconnects magnetic flux at the rational surface to form a helical magnetic island chain. In this paper, it is assumed that $E_{ss} < 0$ so that the m, n tearing mode is intrinsically stable. In this case, any magnetic reconnection that takes place at the rational surface is due solely to the action of the RMP.

The ideal-MHD response of the plasma to the RMP is governed by the dimensionless parameter $E_{sv} = [d\hat{\psi}_v/d\ln r]_{r_s}^{r_{s+}}$, where $\hat{\psi}_v(r)$ is a solution of the marginally stable, ideal-MHD equations, for the case of an m, n helical perturbation, which satisfies physical boundary conditions at $r=0$ and $r=a$, in the presence of the RMP, and is such that $\hat{\psi}_v(r_s) = 0$.¹⁶

D. Linear response regime

In the linear response regime, the reconnected magnetic flux induced by the RMP at the rational surface is governed by^{15,26,27}

$$\frac{\delta_s}{r_s} \tau_R \left(\frac{d}{dt} + i\omega_s \right) \Psi_s = E_{ss} \Psi_s + E_{sv} \Psi_v, \quad (1)$$

where δ_s is the linear layer width, $\tau_R = \mu_0 r_s^2 \sigma(r_s)$ the resistive diffusion timescale, and

$$\omega_s(t) = m \Omega_\theta(r_s, t) - n \Omega_\phi(r_s, t). \quad (2)$$

Here, $\sigma(r)$, $\Omega_\theta(r, t)$, and $\Omega_\phi(r, t)$ are the plasma electrical conductivity, poloidal angular velocity, and toroidal angular velocity profiles, respectively. Note that, in this paper, we are assuming that the constant- ψ approximation¹⁰ holds at the rational surface. (It is demonstrated in Ref. 28 that the appropriate linear response regime for an RMP resonant in the pedestal of a typical DIII-D H-mode discharge is the so-called “first semi-collisional regime,” which is indeed a constant- ψ response regime. Moreover, if the appropriate linear response regime is constant- ψ then so is the appropriate nonlinear response regime, because the constant- ψ constraint is easier to satisfy in the nonlinear regime than in the linear regime.^{26,29})

Equation (1) can be rewritten as an “amplitude evolution equation,”

$$\frac{\delta_s}{r_s} \tau_R \frac{d|\Psi_s|}{dt} = E_{ss} |\Psi_s| + E_{sv} |\Psi_v| \cos(\varphi_s - \varphi_v), \quad (3)$$

combined with a “phase evolution equation,”

$$\frac{d\varphi_s}{dt} = \omega_s - \frac{E_{sv}}{\tau_R} \frac{r_s}{\delta_s} \frac{|\Psi_v|}{|\Psi_s|} \sin(\varphi_s - \varphi_v). \quad (4)$$

The final term on the right-hand side of Eq. (4) is termed the “slip-frequency” and is the difference between the helical phase velocity of the reconnected magnetic flux and that expected on the assumption that the flux is convected by the plasma flow at the rational surface (i.e., $d\varphi_s/dt = \omega_s$). In general, the slip-frequency is non-zero because

the plasma in the vicinity of the rational surface is capable of diffusing resistively through the linear layer structure.

E. Nonlinear response regime

In the nonlinear response regime, Eq. (3) generalizes to the “Rutherford island width evolution equation”:^{12,21}

$$\frac{(\mathcal{I}/2) W_s}{r_s} \tau_R \frac{d|\Psi_s|}{dt} = E_{ss} |\Psi_s| + E_{sv} |\Psi_v| \cos(\varphi_s - \varphi_v), \quad (5)$$

where

$$W_s = 4 \left(\frac{|\Psi_s|}{r_s s(r_s) B_\theta(r_s)} \right)^{1/2} r_s \quad (6)$$

is the full radial width of the magnetic island chain, $\mathcal{I} = 0.8227$, and $s(r) = d \ln q / d \ln r$. The nonlinear regime holds when $W_s \gg \delta_s$, whereas the linear regime holds when $W_s \ll \delta_s$.

Equation (5) is usually coupled with the so-called “no-slip constraint”¹⁵

$$\frac{d\varphi_s}{dt} = \omega_s. \quad (7)$$

The reasoning behind the imposition of this constraint is that plasma is trapped inside the magnetic separatrix of the island chain that forms in the vicinity of the rational surface, which forces the chain to co-rotate with the local plasma flow. However, in reality, the plasma is able to diffuse resistively across the separatrix to some extent. Hence, by analogy with Eqs. (3)–(5), and in accordance with Refs. 22 and 23, in this paper we shall modify Eq. (7) such that

$$\frac{d\varphi_s}{dt} = \omega_s - \frac{E_{sv}}{\tau_R} \frac{r_s}{(\mathcal{I}/2) W_s} \frac{|\Psi_v|}{|\Psi_s|} \sin(\varphi_s - \varphi_v). \quad (8)$$

In effect, we are saying that a nonlinear magnetic island chain acts like a constant- ψ linear layer whose width is $(\mathcal{I}/2) W_s$. The final term on the right-hand side of the previous equation is the “nonlinear slip-frequency.” In general, we would expect this frequency to be relatively small [because it is usually the case that $|\omega_s| \tau_R (W_s/r_s) \gg 1$ for fully developed magnetic islands in high-temperature tokamak plasmas^{23,28}]. Nevertheless, the nonlinear slip-frequency may be non-negligible for developing island chains, which is why we are including it in our analysis.

F. Composite model

If we define $X_s = |\Psi_s| \cos \varphi_s$, $Y_s = |\Psi_s| \sin \varphi_s$, $X_v = |\Psi_v| \cos \varphi_v$, and $Y_v = |\Psi_v| \sin \varphi_v$ then we can combine Eqs. (3)–(5) and (8) to give the following composite resonant response model that interpolates between the linear and the nonlinear regimes:^{22,23,30}

$$\left(\frac{(\mathcal{I}/2) W_s + \delta_s}{r_s} \right) \tau_R \left(\frac{dX_s}{dt} + \omega_s Y_s \right) = E_{ss} X_s + E_{sv} X_v, \quad (9)$$

$$\left(\frac{(\mathcal{I}/2) W_s + \delta_s}{r_s} \right) \tau_R \left(\frac{dY_s}{dt} - \omega_s X_s \right) = E_{ss} Y_s + E_{sv} Y_v, \quad (10)$$

where

$$W_s = 4 \left(\frac{\sqrt{X_s^2 + Y_s^2}}{s_s r_s B_\theta(r_s)} \right)^{1/2} r_s. \quad (11)$$

With the benefit of hindsight, Eqs. (9) and (10) could have been derived more directly from the following heuristic generalization of Eq. (1):²³

$$\left(\frac{(\mathcal{I}/2) W_s + \delta_s}{r_s} \right) \tau_R \left(\frac{d}{dt} + i \omega_s \right) \Psi_s = E_{ss} \Psi_s + E_{sv} \Psi_v. \quad (12)$$

As seems reasonable, the interpolation weights between the linear term δ_s and the nonlinear term $(\mathcal{I}/2) W_s$ in the previous equation have both been chosen to be unity, which ensures that the resonant response model asymptotes to standard constant- ψ linear layer theory in the limit $W_s \ll \delta_s$, and to the Rutherford island width evolution equation combined with a nonlinear finite slip-frequency model in the limit $W_s \gg \delta_s$.

III. EPEC MODEL

A. Introduction

Let us now generalize our investigation to toroidal geometry.

B. Modified toroidal resonant response model

The toroidal model of the response of a tokamak plasma to a static, externally generated, RMP that is implemented in the EPEC code²⁵ is described in detail in Ref. 24. In the light of the composite cylindrical resonant response model developed in Sec. II, we propose to modify the resonant response component of the EPEC model (this component is described in Sec. D of Ref. 24).

Equations (D1) and (D2) in Ref. 24 are modified such that

$$(\hat{W}_k + \hat{\delta}_k) \mathcal{S}_k \frac{d\hat{\Psi}_k}{dt} = \sum_{k'=1,K} \hat{E}_{kk'} \hat{\Psi}_{k'} \cos(\varphi_k - \varphi_{k'} - \xi_{kk'}) + \hat{E}_{kk} \hat{\gamma}_k \cos(\varphi_k - \zeta_k), \quad (13)$$

$$\mathcal{S}_k = \frac{\tau_R(\hat{r}_k)}{\tau_A}, \quad (14)$$

respectively. Here,

$$\hat{W}_k = \frac{2\mathcal{I}}{\hat{a} \hat{r}_k} \left(\frac{q}{g s} \right)_{\hat{r}_k}^{1/2} |\hat{\Psi}_k|^{1/2}, \quad (15)$$

$$\hat{\delta}_k = \frac{\delta_{SC}(\hat{r}_k)}{R_0 \hat{a} \hat{r}_k}, \quad (16)$$

where $\delta_{SC}(\hat{r})$ is the semi-collisional linear layer width specified in Ref. 28.

In the previous expressions, R_0 is the major radius of the magnetic axis, r is a magnetic flux-surface label with dimensions of length (which, roughly speaking, is the average minor radius of the flux-surface), $q(r)$ is the safety-factor profile, $s(r) = d \ln q / d \ln r$, $g(r) B_0$ is the toroidal magnetic field-strength at major radius R_0 , B_0 is the vacuum toroidal magnetic field-strength on the magnetic axis, a is the value of r on the last closed magnetic flux-surface, r_k is the value of r on the k th rational surface (resonant with poloidal mode number m_k , and toroidal mode number n), $\hat{a} = a/R_0$, $\hat{r} = r/a$, and $\hat{r}_k = r_k/a$. Here, K is the number of rational surfaces in the plasma. Furthermore,

$\tau_R(\hat{r}) = \mu_0 r^2 \sigma_{ee}(\hat{r}) Q_{00}^{ee}(\hat{r})$, where σ_{ee} is the classical plasma parallel electrical conductivity, and Q_{00}^{ee} , which is defined in Sec. B of Ref. 24, is a dimensionless parameter that specifies the corrections to this conductivity due to neoclassical effects and the presence of plasma impurities. Also, $\tau_A = [\mu_0 \rho(0) a^2 / B_0^2]^{1/2}$ is a convenient scale time, $\rho(r)$ is the plasma mass density profile, and $\hat{t} = t/\tau_A$. Finally, $\Psi_k = B_0 R_0 \hat{\Psi}_k e^{-i\varphi_k}$ is the reconnected magnetic flux at the k th rational surface, $\chi_k = B_0 R_0 \hat{\chi}_k e^{-i\zeta_k}$ is a measure of the vacuum magnetic flux at the k th rational surface (in fact, $\hat{E}_{kk} \chi_k$ is equivalent to $E_{sv} \Psi_v$ in Sec. II), and $E_{kk'} = \hat{E}_{kk'} e^{-i\zeta_{kk'}}$ is the toroidal tearing stability matrix.¹⁶ Here, $\hat{\Psi}_k > 0$, $\varphi_k, \hat{\chi}_k > 0$, $\zeta_k, \hat{E}_{kk'} > 0$, and $\zeta_{kk'}$ are all real quantities.

Note that the EPEC code calculates the elements of the toroidal tearing mode stability matrix, $E_{kk'}$, making use of a high- q approximation.²⁴ On the other hand, the χ_k , which specify the ideal response of the plasma to the applied RMP, are calculated by the GPEC code.³¹

Equation (13) represents a *minor* improvement to Eq. (D1) of Ref. 24 in which the interpolation between the linear and nonlinear regimes is performed in a slightly more accurate manner. [To be more exact, in Ref. 24, $(\hat{W}_k + \hat{\delta}_k) \mathcal{S}_k$ is effectively replaced by $(\hat{W}_k + h_k \hat{\delta}_k) \mathcal{S}_k$, where $h_k = (2\mathcal{I}/\hat{a})(q/gs)_{\hat{r}_k}^{1/2}$. The additional factor of h_k is spurious. Fortunately, h_k is an $\mathcal{O}(1)$ parameter.]

Equation (D6) of Ref. 24 is modified such that

$$(\hat{W}_k + \hat{\delta}_k) \mathcal{S}_k \left(\frac{d\varphi_k}{dt} - \hat{\omega}_k \right) = - \sum_{k'=1,K} \hat{E}_{kk'} \hat{\Psi}_{k'} \sin(\varphi_k - \varphi_{k'} - \zeta_{kk'}) - \hat{E}_{kk} \hat{\chi}_k \sin(\varphi_k - \zeta_k), \quad (17)$$

where

$$\hat{\omega}_k(\hat{t}) = \hat{\omega}_{k0} - \sum_{k'=1,P} \frac{m_k}{m_{k'}} \frac{y_p(\hat{r}_k)}{y_p(\hat{r}_{k'})} \alpha_{k',p}(\hat{t}) - \sum_{k'=1,K} \frac{z_p(\hat{r}_k)}{z_p(\hat{r}_{k'})} \beta_{k',p}(\hat{t}), \quad (18)$$

$\hat{\omega}_{k0} = \omega_{k0} \tau_A$, $y_p(\hat{r}) = J_1(j_{1,p} \hat{r})/\hat{r}$, and $z_p(\hat{r}) = J_0(j_{0,p} \hat{r})$. Here, ω_{k0} is the so-called “natural frequency” (in the absence of the RMP) at the k th rational surface; this quantity is defined as the helical phase velocity of a naturally unstable island chain, resonant at the surface, in the absence of an RMP (or any other island chains). Furthermore, $J_m(z)$ is a standard Bessel function, and $j_{m,p}$ denotes the p th zero of this function. Finally, P is a positive integer that is much larger than unity.

Equation (17) represents a *major* improvement to Eq. (D6) of Ref. 24 that takes into account the finite slip-frequencies of the magnetic island chains induced at the various rational surfaces in the plasma. In the absence of a finite slip-frequency, the right-hand side of Eq. (17) would be zero.

If we define $X_k = \hat{\Psi}_k \cos \varphi_k$ and $Y_k = \hat{\Psi}_k \sin \varphi_k$, then Eqs. (13) and (17) are more conveniently written in the nonsingular (when $\hat{\Psi}_k = 0$) forms

$$(\hat{W}_k + \hat{\delta}_k) \mathcal{S}_k \left(\frac{dX_k}{dt} + \hat{\omega}_k Y_k \right) = \sum_{k'=1,K} \hat{E}_{kk'} (\cos \zeta_{kk'} X_{k'} - \sin \zeta_{kk'} Y_{k'}) + \hat{E}_{kk} \hat{\chi}_k \cos \zeta_k, \quad (19)$$

$$(\hat{W}_k + \hat{\delta}_k) \mathcal{S}_k \left(\frac{dY_k}{dt} - \hat{\omega}_k X_k \right) = \sum_{k'=1,K} \hat{E}_{kk'} (\cos \zeta_{kk'} Y_{k'} + \sin \zeta_{kk'} X_{k'}) + \hat{E}_{kk} \hat{\chi}_k \sin \zeta_k, \quad (20)$$

where

$$\hat{W}_k = \frac{2\mathcal{I}}{\hat{a} \hat{r}_k} \left(\frac{q}{gs} \right)_{\hat{r}_k}^{1/2} (X_k^2 + Y_k^2)^{1/4}. \quad (21)$$

Equations (19)–(21) are the toroidal generalizations of Eqs. (9)–(11), respectively.

C. Plasma angular velocity evolution

Our system of equations is completed by the time evolution equations for the $\alpha_{k,p}$ and $\beta_{k,p}$ parameters. These equations specify how the plasma poloidal and toroidal angular velocity profiles are modified by the electromagnetic torques that develop within the plasma, in response to the applied RMP, and how these modifications affect the natural frequencies. The evolution equations take the form²⁴

$$(1 + 2q_k^2) \frac{d\alpha_{k,p}}{dt} + \left(\frac{j_{1,p}^2}{\hat{\tau}_{Mk}} + \frac{1}{\hat{\tau}_{0k}} \right) \alpha_{k,p} = \frac{m_k^2 [y_p(\hat{r}_k)]^2}{\hat{\rho}_k \hat{a}^2 [J_2(j_{1,p})]^2} \delta \hat{T}_k, \quad (22)$$

$$\frac{d\beta_{k,p}}{dt} + \frac{j_{0,p}^2}{\hat{\tau}_{Mk}} \beta_{k,p} = \frac{n^2 [z_p(\hat{r}_k)]^2}{\hat{\rho}_k [J_1(j_{0,p})]^2} \delta \hat{T}_k, \quad (23)$$

where

$$\delta \hat{T}_k = \sum_{k'=1,K} \hat{E}_{kk'} \hat{\Psi}_{k'} \hat{\Psi}_k \sin(\varphi_k - \varphi_{k'} - \zeta_{kk'}) + \hat{E}_{kk} \hat{\Psi}_k \hat{\chi}_k \sin(\varphi_k - \zeta_k). \quad (24)$$

Here, $q_k = m_k/n$, $\hat{\rho}_k = \rho(\hat{r}_k)/\rho(0)$, $\hat{\tau}_{Mk} = a^2/[\chi_{\perp\phi}(\hat{r}_k) \tau_A]$, and $\tau_{0k} = \tau_{\theta}(\hat{r}_k)/\tau_A$. Moreover, $\chi_{\perp\phi}(\hat{r}_k)$ is the toroidal perpendicular momentum diffusivity profile, whereas

$$\tau_{\theta}(\hat{r}) = \left[\frac{\hat{r} \hat{a}}{q(\hat{r})} \right]^2 \frac{\tau_{ii}(\hat{r})}{\mu_{00}^i(\hat{r})} \quad (25)$$

is the poloidal flow damping time profile. Finally, τ_{ii} is the classical ion–ion collision time, and μ_{00}^i is a dimensionless neoclassical viscosity parameter that is defined in Sec. B of Ref. 24.

Once the natural frequencies, in the absence of the RMP, have been specified, Eqs. (18) and (19)–(24), form a complete set.

IV. EPEC MODELING OF DIII-D DISCHARGE #145380

A. Introduction

DIII-D discharge #145380 is an ITER-similar-shape (ISS), edge-localized-modeling, H-mode discharge in which the plasma current is slowly ramped in order to scan the magnetic safety-factor.^{32,33} This discharge is described in more detail in Sec. III B of Ref. 25. In addition, Fig. 1 of Ref. 25 gives an overview of the discharge, whereas Figs. 2 and 3 show the plasma equilibrium and the plasma profiles, respectively, at the commencement of the current ramp. A static RMP is applied to the plasma by running steady $n = 3$ currents through the

I-coil system.³⁴ Three windows of ELM suppression are evident in Fig. 1 of Ref. 25: the first occurs when $t \simeq 2900$ ms and $q_{95} \simeq 3.91$; the second occurs when $t = 3400$ ms and $q_{95} \simeq 3.66$; and the third occurs when $t \simeq 4000$ ms and $q_{95} \simeq 3.41$. Here, q_{95} is the safety-factor at the 95% flux-surface.

B. Relaxation of no-slip constraint

As is discussed in Ref. 25, the best agreement between the predictions of the EPEC code and experimental observations is obtained by assuming that the unperturbed natural frequencies at the various rational surfaces in the plasma are determined by the local equilibrium $\mathbf{E} \times \mathbf{B}$ velocity. In other words,

$$\omega_{k0} = -n \omega_E(\hat{r}_k), \quad (26)$$

where $\omega_E(\hat{r}) = -d\Phi/d\Psi_p$. Here, $\Phi(\hat{r})$ is the equilibrium scalar electric potential (in the absence of the RMP), and $\Psi_p(\hat{r})$ the equilibrium poloidal magnetic flux (divided by 2π). Equation (26) holds at every rational surface in both of the simulations discussed in Secs. IV B 1 and IV B 2.

1. No-slip constraint imposed

In our first simulation, the no-slip constraint is imposed at all rational surfaces in the plasma. This implies that the resonant response model at the k th rational surface consists of Eqs. (13) and (17), with the right-hand side of the latter equation set to zero; in other words, the slip-frequency is set to zero at the k th rational surface.

The upper panel of Fig. 1 shows the natural frequencies, in the absence of the RMP, of the various $n = 3$ tearing modes that are resonant in the pedestal of DIII-D discharge #145380, whereas the lower panel of Fig. 1 shows the same frequencies in the presence of the RMP. It is apparent that if the magnitude of the natural frequency in the absence of the RMP falls below about 3 krad/s then the associated tearing mode locks to the RMP (i.e., its true natural frequency becomes zero).

The upper panel of Fig. 2 shows the widths of the various magnetic island chains driven by the applied $n = 3$ RMP in the absence of shielding due to plasma flow, whereas the lower panel shows the same widths in the presence of shielding. It is apparent that the predicted island widths are generally much smaller than the “vacuum” island widths (i.e., the widths in the absence of shielding), as a consequence of the shielding of driven magnetic reconnection by plasma flow. However, this shielding breaks down at various rational surfaces when the associated natural frequency is zero (see the lower panel of Fig. 2). In this situation, the driven island width is similar to the vacuum island width.

According to the prevailing hypothesis, RMP-induced ELM mitigation/suppression in an H-mode tokamak discharge occurs when a comparatively wide, locked, magnetic island chain is generated at the top of the pedestal.^{35,36} The temperature and density flattening associated with the chain is presumed to limit the radial expansion of the pedestal, and, thereby, prevent it from attaining a width sufficient to destabilize peeling-ballooning modes³⁷ (which are thought to trigger ELMs).³²

According to Fig. 2, the comparatively wide, $m = 11$ (brown), $m = 10$ (magenta), and $m = 9$ (cyan), locked magnetic island chains which are predicted to be driven by the RMP in the pedestal of DIII-D discharge #145380 line up fairly well with the first, second, and third,

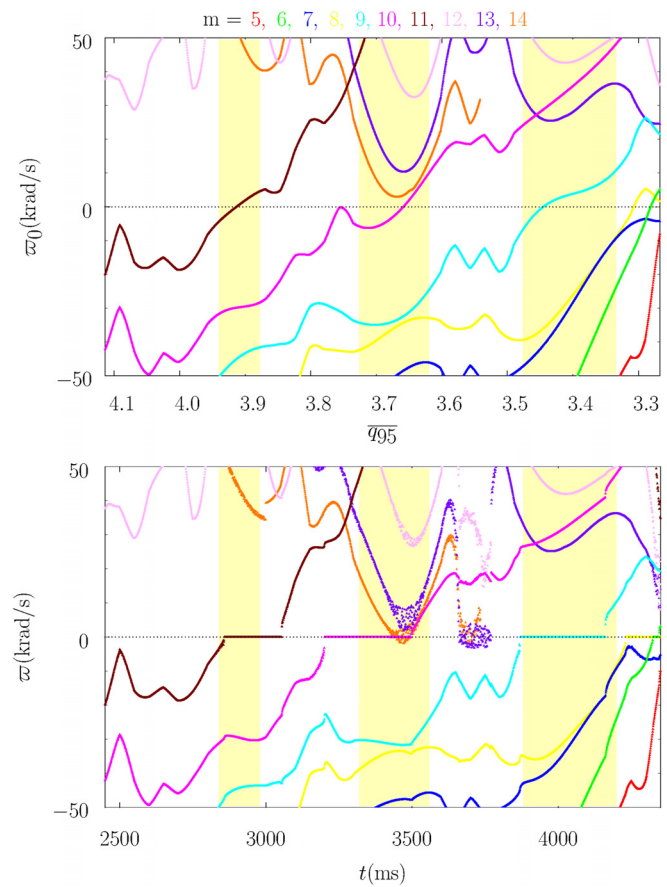


FIG. 1. Composite linear/nonlinear calculation with the no-slip constraint imposed at all rational surfaces, and the natural frequencies in the absence of the RMP determined by the local $\mathbf{E} \times \mathbf{B}$ velocity. Top panel: $n = 3$ natural frequencies, in the absence of RMP, as functions of the least squares linear fit to q_{95} vs time in DIII-D discharge #145380. Bottom panel: $n = 3$ natural frequencies, in the presence of RMP, as functions of time in DIII-D discharge #145380. The red, green, blue, yellow, cyan, magenta, brown, pink, purple, and orange curves correspond to $m = 5, 6, 7, 8, 9, 10, 11, 12, 13$, and 14 , respectively. The yellow vertical bands indicate the ELM-suppression windows.

ELM-suppression windows, respectively. To be more exact, the island chains are located at the top of the pedestal (i.e., $\Psi_N = 0.925$) and also occur in roughly the correct q_{95} ranges. This is consistent with the hypothesis that the formation of locked magnetic island chains at the top of the pedestal causes ELM mitigation/suppression. Here, $\Psi_N(\hat{r}) = [\Psi_p(\hat{r}) - \Psi_p(0)]/[\Psi_p(\hat{a}) - \Psi_p(0)]$ is the conventional normalized equilibrium poloidal magnetic flux.

In principle, the calculation shown in Figs. 1 and 2 is a repeat of one performed in Ref. 25. In practice, there is a slight difference between the two calculations because the expression for the linear layer width used in Eq. (D1) of Ref. 24 (which specifies the island width evolution equation employed in Ref. 25), which was only intended to be approximate, is slightly inaccurate [because it contains a spurious factor of $(2\mathcal{I}/\hat{a})(q/gs)^{1/2}_{\hat{r}_k}$ —see Sec. III A]. This accounts for the very minor differences between Figs. 1 and 2 in this paper and Figs. 8 and 9 in Ref. 25.

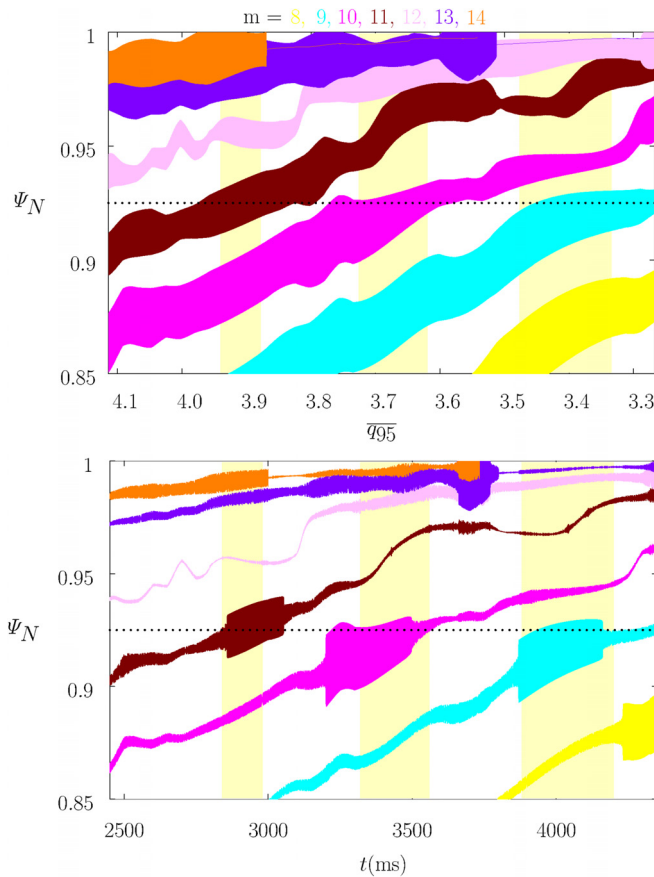


FIG. 2. Composite linear/nonlinear calculation with the no-slip constraint imposed at all rational surfaces, and the natural frequencies in the absence of the RMP determined by the local $\mathbf{E} \times \mathbf{B}$ velocity. Top panel: full $n=3$ vacuum island widths as functions of the least squares linear fit to q_{95} vs time in DIII-D discharge #145380. Bottom panel: full $n=3$ island widths as functions of time in DIII-D discharge #145380. The yellow, cyan, magenta, brown, pink, purple, and orange areas correspond to $m=8, 9, 10, 11, 12, 13$, and 14 , respectively. The yellow vertical bands indicate the ELM-suppression/mitigation windows. The horizontal dotted lines indicate the top of the pedestal, $\Psi_N = 0.925$.

2. No-slip constraint relaxed

In our second simulation, the no-slip constraint is relaxed at all rational surfaces in the plasma. This implies that the resonant response model at the k th rational surface consists of Eqs. (19) and (20). Figures 3 and 4 show analogous data to Figs. 1 and 2, respectively. Figure 5 shows details of the bottom panels of Figs. 1 and 3, in order to better illustrate the island chain dynamics when the RMP-modified natural frequencies of the various $n=3$ tearing modes in plasma are comparatively small.

A comparison of Figs. 1 and 3, as well as an examination of Fig. 5, reveals that the relaxation of the no-slip constraint facilitates the locking of magnetic island chains to the RMP to a relatively modest degree. (Here, by locking, we mean a reduction in the RMP-modified natural frequency to a value close to zero.) This is not surprising because relaxation of the no-slip constraint clearly weakens the coupling between a given magnetic island chain and the local plasma flow (which is ultimately responsible for the

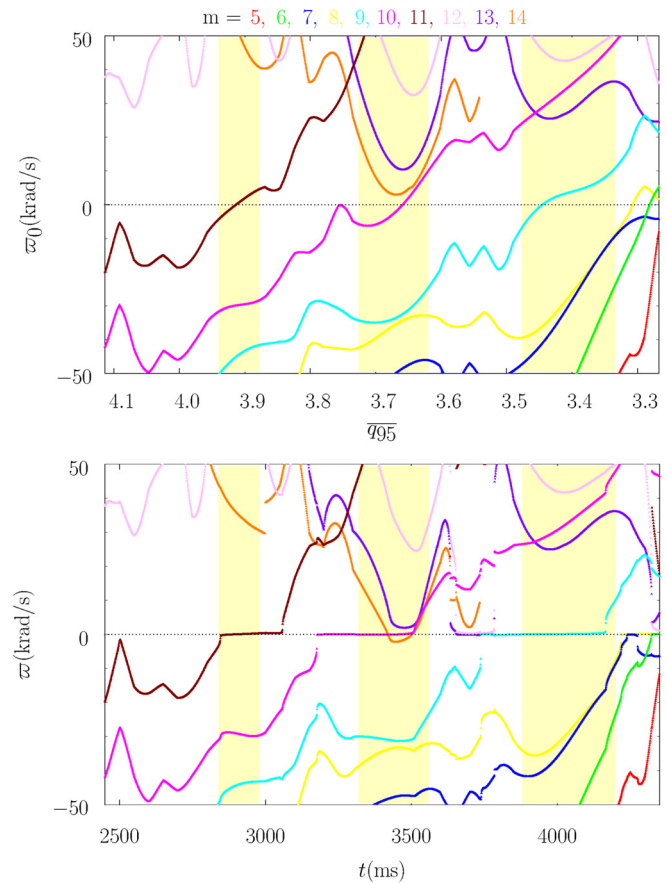


FIG. 3. Composite linear/nonlinear calculation with the no-slip constraint relaxed at all rational surfaces, and the natural frequencies in the absence of the RMP determined by the local $\mathbf{E} \times \mathbf{B}$ velocity. Top panel: $n=3$ natural frequencies, in the absence of RMP, as functions of the least squares linear fit to q_{95} vs time in DIII-D discharge #145380. Bottom panel: $n=3$ natural frequencies, in the presence of RMP, as functions of time in DIII-D discharge #145380. The red, green, blue, yellow, cyan, magenta, brown, pink, purple, and orange curves correspond to $m=5, 6, 7, 8, 9, 10, 11, 12, 13$, and 14 , respectively. The yellow vertical bands indicate the ELM-suppression windows.

shielding of driven magnetic reconnection). It can be seen from Fig. 5 that if the no-slip constraint is imposed, then the RMP-modified natural frequencies of locked magnetic island chains are exactly zero. On the other hand, if the no-slip constraint is relaxed, then locked magnetic island chains possess small but finite RMP-modified natural frequencies, because the local plasma flow is able to slip through the stationary chains to some extent. However, the degree of slippage for a fully developed locked magnetic island chain is comparatively small (i.e., no more than 0.5 krad/s), which helps explain why the no-slip constraint can be used to accurately predict the dynamics of wide magnetic island chains in tokamaks and reversed field pinches.³⁸

It is remarkable that the results shown in Figs. 1–3 are so similar, given that the relaxation of the no-slip constraint leads to a radical modification of the dynamics of non-locked magnetic island chains. When the no-slip constraint is imposed, the widths of magnetic island chains that are unable to lock to the RMP are forced to pulsate,

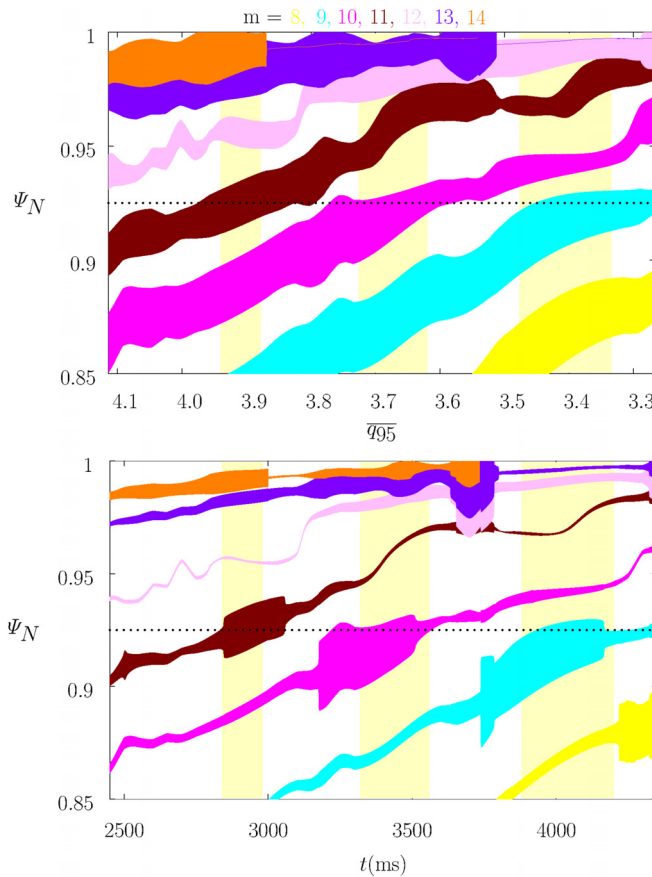


FIG. 4. Composite linear/nonlinear calculation with the no-slip constraint relaxed at all rational surfaces, and the natural frequencies in the absence of the RMP determined by the local $\mathbf{E} \times \mathbf{B}$ velocity. Top panel: full $n = 3$ vacuum island widths as functions of the least squares linear fit to q_{95} vs time in DIII-D discharge #145380. Bottom panel: full $n = 3$ island widths as functions of time in DIII-D discharge #145380. The yellow, cyan, magenta, brown, pink, purple, and orange areas correspond to $m = 8, 9, 10, 11, 12, 13$, and 14 , respectively. The yellow vertical bands indicate the ELM-suppression windows. The horizontal dotted lines indicate the top of the pedestal, $\Psi_N = 0.925$.

periodically falling to zero, because the helical phases of the chains are forced to continuously increase (or decrease) by their non-zero natural frequencies.^{26–28,39} On the other hand, when the no-slip constraint is relaxed, the widths of magnetic island chains that are unable to lock to the RMP have steady values, because the chains can slip with respect to the local plasma flow, which means that they can have fixed helical phases despite the fact that their natural frequencies are non-zero.

Unfortunately, although the relaxation of the no-slip constraint is undoubtedly correct, from a physics standpoint, it does not lead to an obvious improvement in agreement between the predictions of the EPEC model and experimental results.

C. Improved interpolation between linear and nonlinear resonant response regimes

According to linear tearing mode theory, in the absence of the RMP, the natural frequency of the tearing mode resonant at the k th rational surface is given by^{13,40–42}

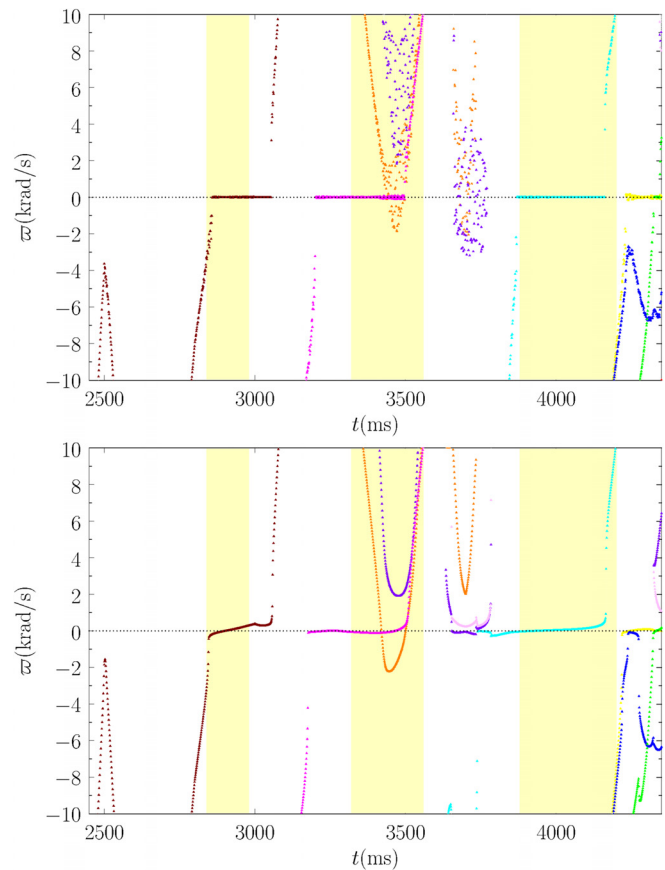


FIG. 5. Top panel: details of the bottom panel of Fig. 1. Bottom panel: details of the bottom panel of Fig. 3.

$$\varpi_{k0} = \varpi_{\ln k} \equiv -n(\omega_E + \omega_{*e})_{\hat{r}_k}, \quad (27)$$

where $\omega_{*e}(\hat{r}) = (T_e/e) d \ln p_e / d \Psi_p$. Here, e is the magnitude of the electron charge, $p_e(\hat{r})$ the equilibrium (i.e., in the absence of the RMP) electron pressure, and $T_e(\hat{r})$ the equilibrium electron temperature.

According to nonlinear tearing mode theory, in the absence of the RMP, the natural frequency of the tearing mode resonant at the k th rational surface is given by²⁴

$$\varpi_{k0} = \varpi_{\ln k} \equiv -n \left(\omega_E + \left[1 - L_{00}^{ii} + L_{01}^{ii} \left(\frac{\eta_i}{1 + \eta_i} \right) \right] \omega_{*i} - \left[L_{00}^{il} - L_{01}^{il} \left(\frac{\eta_I}{1 + \eta_I} \right) \right] \omega_{*I} \right)_{\hat{r}_k}, \quad (28)$$

where $\omega_{*a}(\hat{r}) = -(T_a/Z_a e) d \ln p_a / d \Psi_p$, $\eta_a(\hat{r}) = d \ln T_a / d \ln n_a$, for $a = i, I$. Here, Z_b , n_b , T_b , $p_I = n_I T_I$ are the charge number, equilibrium number density, equilibrium temperature, and equilibrium pressure of the majority (thermal) ions, respectively, whereas Z_b , n_b , T_b , $p_I = n_I T_I$ are the corresponding quantities for the impurity ions. Furthermore, $L_{00}^{ii}(\hat{r})$, $L_{01}^{ii}(\hat{r})$, $L_{00}^{il}(\hat{r})$, and $L_{01}^{il}(\hat{r})$ are dimensionless neoclassical parameters that are defined in Sec. B of Ref. 24.

Finally, the best agreement between theory and experiment is obtained by assuming that, in the absence of the RMP, the natural frequency of the tearing mode resonant at the k th rational surface is given by Eq. (26).^{25,43}

1. Linear calculation

For the sake of comparison, we shall first perform a purely linear calculation. Thus, the resonant plasma response model at the k th rational surface consists of Eqs. (19) and (20), with \tilde{W}_k set to zero. Moreover, in the absence of the RMP, the natural frequency at the k th rational surface is specified by Eq. (27). Figures 6 and 7 show the natural frequencies in the absence, and in the presence, of the RMP, as well as the vacuum islands widths and the actual island widths.

It can be seen by a comparison between Figs. 1–4, on the one hand, and Figs. 6 and 7, on the other, that the linear calculation

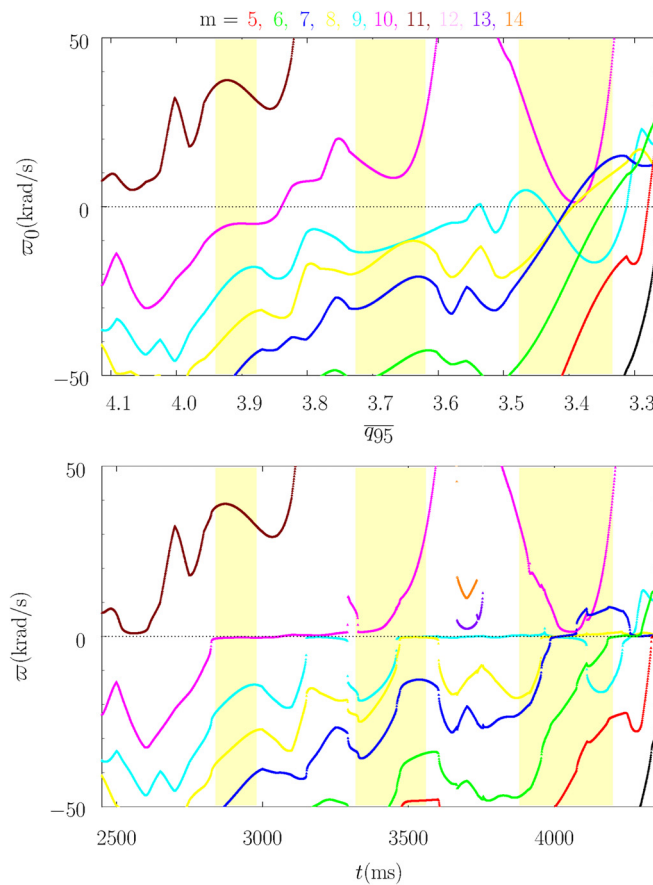


FIG. 6. Linear calculation with the no-slip constraint relaxed at all rational surfaces, and the natural frequencies in the absence of the RMP determined by linear theory. Top panel: $n = 3$ natural frequencies, in the absence of RMP, as functions of the least squares linear fit to q_{95} vs time in DIII-D discharge #145380. Bottom panel: $n = 3$ natural frequencies, in the presence of RMP, as functions of time in DIII-D discharge #145380. The red, green, blue, yellow, cyan, magenta, brown, pink, purple, and orange curves correspond to $m = 5, 6, 7, 8, 9, 10, 11, 12, 13$, and 14 , respectively. The yellow vertical bands indicate the ELM-suppression windows.

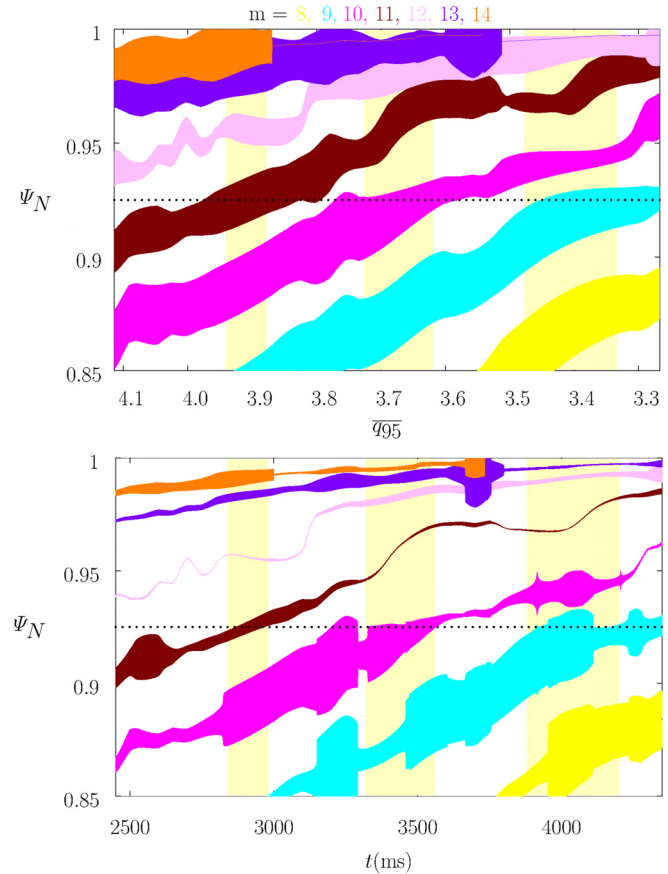


FIG. 7. Linear calculation with the no-slip constraint relaxed at all rational surfaces, and the natural frequencies in the absence of the RMP determined by linear theory. Top panel: full $n = 3$ vacuum island widths as functions of the least squares linear fit to q_{95} vs time in DIII-D discharge #145380. Bottom panel: full $n = 3$ island widths as functions of time in DIII-D discharge #145380. The yellow, cyan, magenta, brown, pink, purple, and orange areas correspond to $m = 8, 9, 10, 11, 12, 13$, and 14 , respectively. The yellow vertical bands indicate the ELM-suppression windows. The horizontal dotted lines indicate the top of the pedestal, $\Psi_N = 0.925$.

very significantly overestimates how easy it is for magnetic island chains to lock to the RMP. We can say this because the $m = 9$ (cyan) magnetic island chain, for example, in the lower panel of Fig. 7 exhibits virtually no shielding due to plasma flow over a wide range of different q_{95} values. The reason for the lack of effective flow shielding is that the linear slip-frequency is comparatively high, because the linear layer width is comparatively narrow, which greatly facilitates the locking of magnetic island chains to the RMP. However, the true slip-frequency becomes less than the linear slip-frequency as soon as the island width exceeds the linear layer width.

2. Composite linear/nonlinear calculation

In our composite linear/nonlinear calculation, the resonant plasma response model at the k th rational surface consists of Eqs. (19)

and (20). Moreover, in the absence of the RMP, the natural frequency at the k th rational surface is specified by

$$\omega_{k0} = \frac{\omega_{\ln k} + (\omega_{\text{ebk}} - \omega_{\ln k} - \omega_{\text{nlk}})x_k + \omega_{\text{nlk}}x_k^2}{1 - x_k + x_k^2}, \quad (29)$$

where $x_k = \hat{W}_k/\hat{\delta}_k$. It follows that $\omega_{k0} = \omega_{\ln k}$ in the linear regime, $x_k \ll 1$; $\omega_{k0} = \omega_{\text{nlk}}$ in the nonlinear regime, $x_k \gg 1$; and $\omega_{k0} = \omega_{\text{ebk}}$ when $x_k = 1$. (Note that ω_{ebk} generally lies between $\omega_{\ln k}$ and ω_{nlk} .) Figures 8 and 9 show the natural frequencies in the absence, and in the presence, of the RMP, as well as the vacuum islands widths and the actual island widths.

It can be seen that the results of the composite linear/nonlinear simulation shown in Figs. 8 and 9 are similar to the results of the nonlinear simulations shown in Figs. 1–4, but significantly different to the results of the linear simulation shown in Figs. 6 and 7. In particular, the composite simulations and the nonlinear

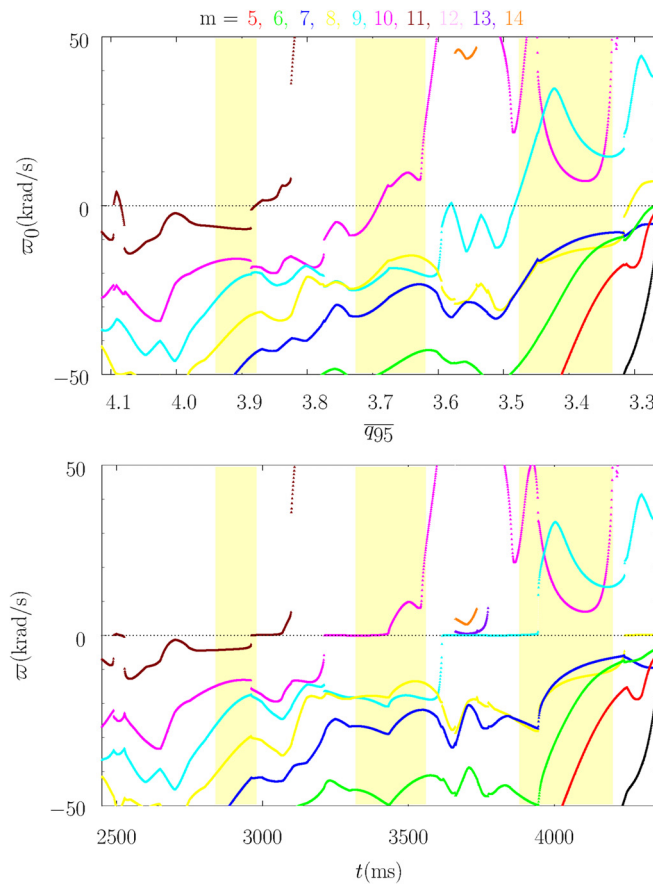


FIG. 8. Composite linear/nonlinear calculation with the no-slip constraint relaxed at all rational surfaces, and the natural frequencies in the absence of the RMP determined by composite linear/nonlinear theory. Top panel: $n=3$ natural frequencies, in the absence of RMP, as functions of the least squares linear fit to q_{95} vs time in DIII-D discharge #145380. Bottom panel: $n=3$ natural frequencies, in the presence of RMP, as functions of time in DIII-D discharge #145380. The red, green, blue, yellow, cyan, magenta, brown, pink, purple, and orange curves correspond to $m=5, 6, 7, 8, 9, 10, 11, 12, 13$, and 14 , respectively. The yellow vertical bands indicate the ELM-suppression windows.

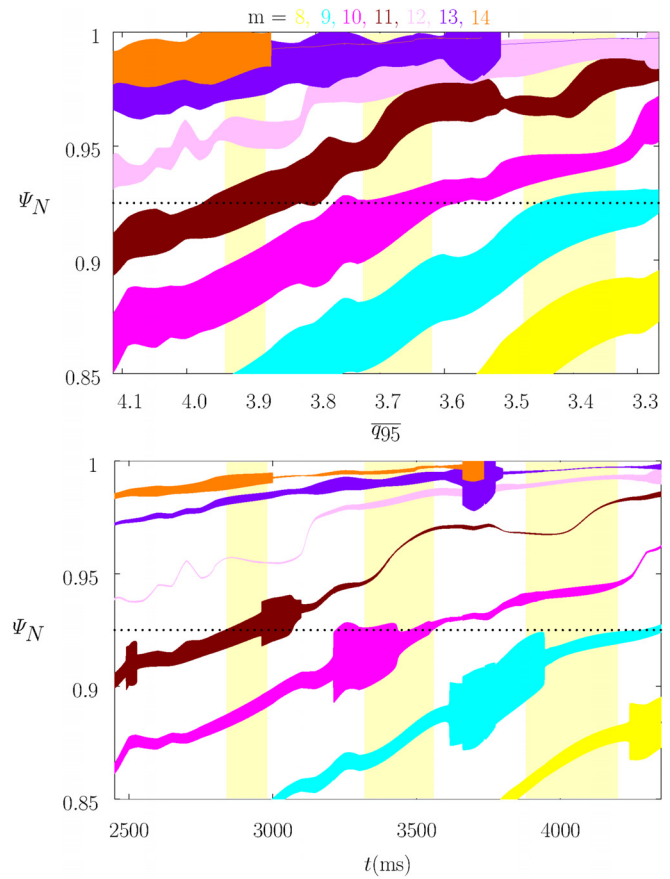


FIG. 9. Composite linear/nonlinear calculation with the no-slip constraint relaxed at all rational surfaces, and the natural frequencies in the absence of the RMP determined by composite linear/nonlinear theory. Top panel: full $n=3$ vacuum island widths as functions of the least squares linear fit to q_{95} vs time in DIII-D discharge #145380. Bottom panel: full $n=3$ island widths as functions of time in DIII-D discharge #145380. The yellow, cyan, magenta, brown, pink, purple, and orange areas correspond to $m=8, 9, 10, 11, 12, 13$, and 14 , respectively. The yellow vertical bands indicate the ELM-suppression windows. The horizontal dotted lines indicate the top of the pedestal, $\Psi_N = 0.925$.

simulations indicate that a magnetic island chain can only lock to the RMP when the magnitude of its natural frequency falls below about 3 krad/s, whereas the linear simulations indicate that locking can occur when the magnitude of the natural frequency falls below about 6 krad/s. The fact that the composite calculation is much more similar to the nonlinear simulation, and significantly different to the linear simulation, confirms the conclusion reached in Ref. 28 that the response of a typical H-mode tokamak plasma to an RMP is not governed by linear theory, because the driven island widths exceed the very narrow linear layer widths, even when driven reconnection is strongly suppressed by plasma flow.

Intriguingly, the composite linear/nonlinear model fairly accurately predicts the widths of the three ELM mitigation/suppression windows in q_{95} (assuming that the windows correspond to the formation of wide locked magnetic island chains at the top of the pedestal). However, the windows are not centered on the correct q_{95} values. We conclude that Eq. (26) gives a more accurate prediction for the natural

frequencies, in the absence of the RMP, than Eq. (29) (because the former equation leads to windows that are centered on the correct q_{95} values). There are a number of possible explanations for this discrepancy. First, the nonlinear tearing mode theory which leads to the prediction (28) for the unperturbed natural frequency of a nonlinear island chain may be missing an important element. (For example, kinetic effects,⁴³ or the influence of neoclassical toroidal flow damping.) Second, the errors in the experimental data, and, in particular, the errors in the experimental $\mathbf{E} \times \mathbf{B}$ velocity profile, may be too large for EPEC to calculate the unperturbed natural frequencies with sufficient precision to accurately determine the locations of the ELM suppression windows in q_{95} space.

V. SUMMARY

We have developed an improved resonant plasma response model that more accurately captures the physics of the interaction between a tokamak plasma and an RMP. The model interpolates between the linear and the nonlinear response regimes and takes into account the fact that the slip-frequency is non-zero in the nonlinear regime. Our improved model has been incorporated into the EPEC toroidal asymptotic matching code.²⁵ The modified EPEC code is used to model RMP-induced ELM mitigation/suppression in DIII-D H-mode discharge #145380.

We find that allowing for a finite slip-frequency (i.e., relaxing the so-called no-slip constraint) slightly facilitates the locking of driven magnetic island chains to the RMP. (Here, by locking, we mean the reduction of the RMP-modified natural frequency of a given chain to a value that is very close to zero.) In fact, there is surprisingly little difference between EPEC simulations that impose the no-slip constraint at the various rational surfaces in the plasma and those in which the constraint is relaxed. This is true despite the fact that the nature of non-locked island solutions is *radically* different in the two cases (in the first case, the widths of the island chains driven at the rational surfaces pulsate, in the second they remain steady).

Our calculations confirm the conclusion reached in Ref. 28 that the response of a typical H-mode tokamak plasma to an RMP cannot be accurately modeled by linear theory. Our calculations also confirm the conclusion reached in Ref. 25 that the best agreement between theory and observations is obtained by assuming that the natural frequencies of tearing modes, in the absence of the RMP, are determined by the local $\mathbf{E} \times \mathbf{B}$ velocity.

None of the improvements to the EPEC model described in this paper lead to markedly better agreement between the predictions of the model and experimental results. In fact, it is clear that the component of the model that has, by far, the most influence on the level of agreement with experimental results is the calculation of the natural frequencies of tearing modes in the absence of the RMP. This suggests that there may be a missing element in this calculation; for example, kinetic effects,⁴³ or the influence of neoclassical toroidal flow damping. Another possibility is that the errors in the experimental data, and, in particular, the errors in the experimental $\mathbf{E} \times \mathbf{B}$ velocity profile, may be too large for the EPEC model to calculate unperturbed natural frequencies with sufficient precision to accurately determine the locations of ELM-suppression windows in q_{95} space. Further detailed comparisons between the predictions of the model and experimental results from a wide range of different H-mode plasmas in different machines may help to further characterize the source of the disagreement.

This report was prepared as an account of work sponsored by an agency of the United States Government. Neither the United States Government nor any agency thereof, nor any of their employees, makes any warranty, express or implied, or assumes any legal liability or responsibility for the accuracy, completeness, or usefulness of any information, apparatus, product, or process disclosed, or represents that its use would not infringe privately owned rights. Reference herein to any specific commercial product, process, or service by trade name, trademark, manufacturer, or otherwise does not necessarily constitute or imply its endorsement, recommendation, or favoring by the United States Government or any agency thereof. The views and opinions of authors expressed herein do not necessarily state or reflect those of the United States Government or any agency thereof.

ACKNOWLEDGMENTS

This research was directly funded by the U.S. Department of Energy, Office of Science, Office of Fusion Energy Sciences, under Contract No. DE-FG02-04ER54742, and incorporates work funded by the U.S. Department of Energy, Office of Science, Office of Fusion Energy Sciences, using the DIII-D National Fusion Facility, a DOE Office of Science user facility, under Contract No. DE-FC02-04ER54698.

DATA AVAILABILITY

The data that support the findings of this study are available from the corresponding author upon reasonable request.

REFERENCES

1. T. Scoville and R. J. LaHaye, *Nucl. Fusion* **43**, 250 (2003).
2. J.-K. Park, M. J. Schaffer, J. E. Menard, and A. H. Boozer, *Phys. Rev. Lett.* **99**, 195003 (2007).
3. N. M. Ferraro, J.-K. Park, C. E. Myers, A. Brooks, S. P. Gerhardt, J. E. Menard, S. Munaretto, and M. L. Reinke, *Nucl. Fusion* **59**, 086021 (2019).
4. T. E. Evans, R. A. Moyer, J. G. Watkins, P. R. Thomas, T. H. Osborne, J. A. Boedo, M. E. Fenstermacher, K. H. Finken, R. J. Groebner, M. Groth *et al.*, *Phys. Rev. Lett.* **92**, 235003 (2004).
5. Y. Liang, H. R. Koslowski, P. R. Thomas, E. Nardon, B. Alper, P. Andrew, Y. Andrew, G. Arnoux, Y. Baranov, M. Bécoulet *et al.*, *Phys. Rev. Lett.* **98**, 265004 (2007).
6. W. Suttrop, T. Eich, J. C. Fuchs, S. Günter, A. Janzer, A. Herrmann, A. Kallenbach, P. T. Lang, T. Lunt, M. Maraschek *et al.*, *Phys. Rev. Lett.* **106**, 225004 (2011).
7. Y. M. Jeon, J.-K. Park, S. W. Yoon, W. H. Ko, S. G. Lee, K. D. Lee, G. S. Yun, Y. U. Nam, W. C. Kim, J.-G. Kwak, K. S. Lee, H. K. Kim, H. L. Yang *et al.*, *Phys. Rev. Lett.* **109**, 035004 (2012).
8. A. Kirk, I. T. Chapman, Y. Liu, P. Cahyna, P. Denner, G. Fishpool, C. J. Ham, J. R. Harrison, Y. Liang, E. Nardon, S. Saarelma, R. Scannell, A. J. Thornton, and MAST Team, *Nucl. Fusion* **53**, 043007 (2013).
9. T. Sun, Y. Liang, Y. Q. Liu, S. Gu, X. Yang, W. Guo, T. Shi, M. Jia, L. Wang, B. Lyu *et al.*, *Phys. Rev. Lett.* **117**, 115001 (2016).
10. H. P. Furth, J. Killeen, and M. N. Rosenbluth, *Phys. Fluids* **6**, 459 (1963).
11. B. Coppi, J. M. Greene, and J. L. Johnson, *Nucl. Fusion* **6**, 101 (1966).
12. P. H. Rutherford, *Phys. Fluids* **16**, 1903 (1973).
13. G. Ara, B. Basu, B. Coppi, G. Laval, M. N. Rosenbluth, and B. V. Waddell, *Ann. Phys.* **112**, 443 (1978).
14. A. Pletzer and R. L. Dewar, *J. Plasma Phys.* **45**, 427 (1991).
15. R. Fitzpatrick, *Nucl. Fusion* **33**, 1049 (1993).
16. R. Fitzpatrick, R. J. Hastie, T. J. Martin, and C. M. Roach, *Nucl. Fusion* **33**, 1533 (1993).
17. S. Tokuda, *Nucl. Fusion* **41**, 1037 (2001).

- ¹⁸D. P. Brennan, R. J. La Haye, A. D. Turnbull, M. S. Chu, T. H. Jensen, L. L. Lao, T. C. Luce, P. A. Politzer, and E. J. Strait, *Phys. Plasmas* **10**, 1643 (2003).
- ¹⁹A. H. Glasser, Z. R. Wang, and J.-K. Park, *Phys. Plasmas* **23**, 112506 (2016).
- ²⁰R. Fitzpatrick, *Phys. Plasmas* **24**, 072506 (2017).
- ²¹P. H. Rutherford, in *Basic Physical Processes of Toroidal Fusion Plasmas: Proceedings of the Course and Workshop, Varenna, 1985* (Commission of the European Communities, Brussels, 1985), Vol. 2, p. 531.
- ²²L. G. Eliseev, N. V. Ivanov, A. M. Kakurin, A. V. Melnikov, and S. V. Perfilov, *Phys. Plasmas* **22**, 052504 (2015).
- ²³W. Huang and P. Zhu, *Phys. Plasmas* **27**, 022514 (2020).
- ²⁴R. Fitzpatrick and A. O. Nelson, *Phys. Plasmas* **27**, 072501 (2020).
- ²⁵R. Fitzpatrick, *Phys. Plasmas* **27**, 102511 (2020).
- ²⁶R. Fitzpatrick, *Phys. Plasmas* **5**, 3325 (1998).
- ²⁷R. Fitzpatrick, *Phys. Plasmas* **21**, 092513 (2014).
- ²⁸R. Fitzpatrick, *Phys. Plasmas* **27**, 042506 (2020).
- ²⁹R. Fitzpatrick, *Phys. Plasmas* **10**, 2304 (2003).
- ³⁰A. N. Chudnovskiy, Y. V. Gvozdkov, N. V. Ivanov, A. M. Kakurin, A. A. Medvedev, I. I. Orlovskiy, Y. D. Pavlov, V. V. Piterskiy, V. D. Pustovitov, M. B. Safonova, V. V. Volkov, and the T-10 Team, *Nucl. Fusion* **43**, 681 (2003).
- ³¹J.-K. Park and N. C. Logan, *Phys. Plasmas* **24**, 032505 (2017).
- ³²P. B. Snyder, T. H. Osbourne, K. H. Burrell, R. J. Groebner, A. W. Leonard, R. Nazikian, D. M. Orlov, O. Schmitz, M. R. Wade, and H. R. Wilson, *Phys. Plasmas* **19**, 056115 (2012).
- ³³Q. M. Hu, R. Nazikian, B. A. Grierson, N. C. Logan, D. M. Orlov, C. Paz-Soldan, and Q. Yu, *Phys. Rev. Lett.* **125**, 045001 (2020).
- ³⁴G. L. Jackson, P. M. Anderson, J. Bialek, W. P. Cary, G. L. Campbell, A. M. Garofalo, R. Hatcher, A. G. Kellman, R. J. LaHaye, A. Nagy *et al.*, in *Proceedings of the 30th EPS Conference on Controlled Fusion and Plasma Physics*, St. Petersburg, Russia (2003), CD-ROM, p. P-4.47.
- ³⁵Q. M. Hu, R. Nazikian, B. A. Grierson, N. C. Logan, J.-K. Park, C. Paz-Soldan, and Q. Yu, *Phys. Plasmas* **26**, 120702 (2019).
- ³⁶Q. M. Hu, R. Nazikian, B. A. Grierson, N. C. Logan, C. Paz-Soldan, and Q. Yu, *Nucl. Fusion* **60**, 076001 (2020).
- ³⁷J. W. Connor, R. J. Hastie, H. R. Wilson, and R. L. Miller, *Phys. Plasmas* **5**, 2687 (1998).
- ³⁸B. E. Chapman, R. Fitzpatrick, D. Craig, P. Martin, and G. Spizzo, *Phys. Plasmas* **11**, 2156 (2004).
- ³⁹R. Fitzpatrick, *Phys. Plasmas* **25**, 112505 (2018).
- ⁴⁰M. Bécoulet, F. Orain, P. Maget, N. Mellet, X. Garbet, E. Nardon, G. T. A. Huysmans, T. Caspar, A. Loarte, P. Cayna *et al.*, *Nucl. Fusion* **52**, 054003 (2012).
- ⁴¹N. M. Ferraro, *Phys. Plasmas* **19**, 056105 (2012).
- ⁴²F. Orain, M. Bécoulet, G. Dif-Pradalier, G. T. A. Huysmans, S. Pamela, E. Nardon, C. Passeron, G. Latu, V. Grandgirard, A. Fil *et al.*, *Phys. Plasmas* **20**, 102510 (2013).
- ⁴³M. F. Heyn, I. B. Ivanov, S. V. Kasilov, W. Kernbichler, I. Joseph, R. A. Moyer, and A. M. Runov, *Nucl. Fusion* **48**, 024005 (2008).